



HAL
open science

Use of DBD plasma, photocatalysis, and combined DBD plasma/photocatalysis in a continuous annular reactor for isovaleraldehyde elimination - Synergetic effect and byproducts identification

Aymen Amine Assadi, Abdelkrim Bouzaza, Cédric Vallet, Dominique Wolbert

► To cite this version:

Aymen Amine Assadi, Abdelkrim Bouzaza, Cédric Vallet, Dominique Wolbert. Use of DBD plasma, photocatalysis, and combined DBD plasma/photocatalysis in a continuous annular reactor for isovaleraldehyde elimination - Synergetic effect and byproducts identification. *The Chemical Engineering Journal*, 2014, 254, pp.124-132. 10.1016/j.cej.2014.05.101 . hal-01063542

HAL Id: hal-01063542

<https://hal.science/hal-01063542>

Submitted on 7 Oct 2014

HAL is a multi-disciplinary open access archive for the deposit and dissemination of scientific research documents, whether they are published or not. The documents may come from teaching and research institutions in France or abroad, or from public or private research centers.

L'archive ouverte pluridisciplinaire **HAL**, est destinée au dépôt et à la diffusion de documents scientifiques de niveau recherche, publiés ou non, émanant des établissements d'enseignement et de recherche français ou étrangers, des laboratoires publics ou privés.

1 **Use of DBD plasma, photocatalysis, and combined DBD**
2 **plasma/photocatalysis in a continuous annular reactor for isovaleraldehyde**
3 **elimination – synergetic effect and byproducts identification**

4
5 Aymen Amine ASSADI ^{a,b}, Abdelkrim BOUZAZA ^{a,b*}, Cédric VALLET ^c, Dominique WOLBERT ^{a,b},

6 ^a Laboratoire Sciences Chimiques de Rennes - équipe Chimie et Ingénierie des Procédés, UMR 6226 CNRS,
7 ENSCR, 11 allée de Beaulieu, CS 50837, 35700 Rennes, France.

8 ^b Université Européenne de Bretagne, Rennes, France

9 ^c Ahlstrom Research and Services, ZI de l'Abbaye - Impasse Louis Champin - 38780 Pont-Evêque, France

10 * Corresponding author. Tel.: +33 2 23238056; fax: +33 2 23238120.

11 E-mail address: Abdelkrim.bouzaza@ensc-rennes.fr (A. Bouzaza).

12
13 **Abstract**

14
15 Removal of isovaleraldehyde from air was investigated experimentally by three processes:
16 dielectric barrier discharge (DBD) plasma, photocatalysis and a DBD plasma/photocatalysis
17 combination. The latter led to a synergetic effect.

18 Many operating parameters were investigated in this study such as the specific energy of
19 discharge, the inlet concentration of isovaleraldehyde and the relative humidity. The UV light
20 generated by the DBD plasma reactor did not activate the photocatalytic medium. Thus, its
21 contribution to the removal of isovaleraldehyde by photocatalysis could be ignored. On the
22 other hand, the use of external UV light significantly improved the removal efficiency.

23 Using a photocatalytic reactor in the presence of water vapor, in small amounts, had a
24 promoting effect on the degradation due to the formation of OH[•] radicals. The same
25 phenomenon has been observed in other processes for small amounts of water in air.

26 The identified and analyzed byproducts were classified into four groups: intermediate
27 products (propionic acid, acetic acid and acetone), carbon monoxide, carbon dioxide and
28 ozone. The carbon balance on carbon products was achieved at about 90%.

29

30 **Keywords:**

31

32 Continuous reactor; synergetic effect; plasma-photocatalysis process; VOC removal;
33 byproduct identification

34

35 **1. Introduction**

36

37 Odor pollution control is an important and challenging issue in the world. Therefore, the
38 treatment of air pollutants has been widely studied during recent years [1]. Air pollution has
39 become a major public concern in the last few decades. The main substances causing odor
40 pollution are sulfur compounds (mercaptans, sulfides), nitrogen compounds (amines and
41 ammonia), and many volatile organic compounds (VOCs) (fatty acids, aldehydes, ketones,
42 alcohols, etc.) [2]. Many industries have seen their gas emissions controlled and limited for
43 environmental reasons. Since 1979, each international protocol has fixed new regulations and
44 gradually reduced the emission limit of major pollutants [3].

45 To solve this problem, research has been conducted to find cost-effective approaches to
46 reduce odor emissions [4, 5]. As a result, many conventional techniques have been proposed
47 to remove VOCs, such as ozone oxidation [6], incineration [3] and photocatalysis [7]. This
48 latter process is a promising air purification technology for trace contaminants because it can
49 degrade a wide range of VOCs to H₂O and CO₂ at room temperature and atmospheric
50 pressure [8].

51 Recently, non-thermal plasma (NTP) has been investigated by many researchers for various
52 applications such as methanol synthesis [9], and hydrogen generation [10]. For environmental
53 applications, NTP is used for surface sterilization in order to eliminate bacteria [11], for water
54 treatment, and for controlling hazardous air pollutants emitted from solvents, paints,
55 automobile exhaust gas, etc. [12-14]

56 In addition, a variety of dielectric barrier discharge (DBD) plasma reactors have been used for
57 the destruction of various VOCs [15-21]. The use of a catalyst in the plasma zone has been
58 reported to improve the efficiency of VOC removal [22]. Moreover, a synergetic effect can be
59 expected when combining volumic plasma with a photocatalyst [21, 22]. On the other hand,
60 Ochiai and co-workers investigated and developed a photocatalysis-plasma hybrid air-
61 purification reactor using a titanium mesh sheet modified with TiO_2 (TMiPTM) and a surface
62 discharge-induced plasma (SPCP) unit [20]. In present study, a novel photocatalysis-plasma
63 hybrid is established in a pilot reactor to investigate the influence of some operating parameters
64 on the removal of VOCs in atmospheric conditions. In our system, the surface dielectric barrier
65 type, is generated by a helicoidally wire electrode which maintain the photocatalyst on the inner
66 wall of the reactor, so that the plasma can be formed directly on the surface of the photocatalyst
67 whereas it was simultaneously illuminated by the external UV radiation.

68 The removal efficiency of isovaleraldehyde by photocatalysis (using external UV) and plasma
69 are tested separately. Isovaleraldehyde (ISOVAL) was chosen since this pollutant is the main
70 molecule detected in the exhaust gases from animal quartering centers.

71 In this paper, the ISOVAL byproducts are identified and evaluated with DBD plasma,
72 photocatalysis and a DBD plasma/photocatalysis combination. In addition, a possible pathway
73 is proposed.

74

75 **2. Experimental set-up and conditions**

76

77 The DBD plasma pilot used (Fig. 1.a) consists of two concentric cylinders ($\text{\O} 58$ and
78 76 mm). To generate the DBD plasma, the reactor is covered by a copper grid, which
79 constitutes the outer electrode. The inner electrode is made from a continuous aluminum
80 helix. It is a 2-mm-thick wire electrode, shaped like a coiled spring (12 turns in 250 mm), in
81 close contact with the inner wall of the reactor. The dielectric medium, the glass reactor wall,
82 is 4 mm in thickness (Fig. 1.b). The high electric voltage applied is about 30 kV/40 mA and is
83 a sine waveform. It is delivered by a high voltage amplifier (TREK_30 kV model 30/20A,
84 USA) coupled with a voltage generator (BFI OPTILAS, France). The outer electrode is
85 connected to the ground through a 2.5 nF capacity. The high voltage applied and the voltage
86 across the capacity are visualized using a digital oscilloscope (Lecroy Wave Surfer 24 Xs, 200
87 MHz) (Fig. 1.b).

88 The catalytic material, provided by Ahlstrom [23], consists of a Glass Fiber Tissue (GFT)
89 coated with 13 g.m^{-2} of colloidal silica to ensure the fixation of 13 g.m^{-2} of titanium dioxide
90 nanoparticles (PC500 Millennium). The coating process involves impregnating the glass
91 fibers with a SiO_2 and TiO_2 nanoparticle suspension in pure water. The preparation process is
92 described in detail in the Ahlstrom Patent [23]. The specific surface area was measured
93 according to the BET method and is equal to $20.6 \text{ m}^2.\text{g}^{-1}$. This material has a thickness of 2
94 mm. The GFT is maintained on the inner reactor wall by the wire electrode (see Fig. 1.b) so
95 that plasma is generated directly on the catalyst surface. The light source is an 80 W UV lamp
96 with a major wavelength peak emission at 360 nm (Philips CLEO performance). The light
97 tube, 1.5 m in length, is placed in the inner concentric cylinder (Fig. 1.b). The UV intensity,
98 which is measured by a UV radiometer (VLX-3W equipped with a sensor CX 365, ALYS
99 Technologies, Switzerland) at the photocatalyst surface, is equal to $20 \pm 3 \text{ W.m}^{-2}$.

100 The design of this reactor (Fig. 1.b) is the subject of a French Patent Application [24].

101 Two sampling points, sealed with a septum, are used to analyze the inlet and outlet gas
102 composition of the reactor. The main air flow can be generated by the internal network of
103 compressed air when dry air is needed (maximum $2 \text{ m}^3 \cdot \text{h}^{-1}$ at 5% relative humidity) or by
104 using ambient air when working at a higher flow rate. The compressed air network enables
105 moisture to be controlled by varying the flow in a packed air-water countercurrent
106 column. Thus, it is possible to obtain a range of relative humidity (RH) from 5 to 90%. The
107 pollutant (ISOVAL) is injected into the inlet air through a syringe pump with a manual refill
108 and a volume of 5 mL. A Venturi system is installed to improve the homogenization of the
109 contaminated air before it is introduced into the reactor. A gas chromatograph coupled with a
110 flame ionization detector (GC Thermo Focus, USA) is used to evaluate the inlet-outlet
111 isovaleraldehyde concentration. ISOVAL and byproduct separation are performed by a
112 Chrompack FFAP-CB column (25 m in length, external diameter of 0.32 mm), which is
113 specially adapted for volatile fatty acids. Nitrogen gas is the mobile phase. Byproducts are
114 identified by a Gas Chromatograph-Mass Spectrometer (GC-MS) (Thermo Scientific)
115 equipped with an infrared (IR) detector. All injections are performed manually and repeated
116 three times with a syringe of 500 μl . Analysis conditions are as follows (Table 1).

117

118 **Table 1: Analysis conditions for the gas chromatograph**

119

120 The CO concentrations are measured by an NO/CO ZRE gas analyzer while CO₂ is analyzed
121 by a Transform Infrared Fourier (FTIR) spectrophotometer from Environnement SA (Cosma
122 Beryl reference 100). The measurement accuracy is 5%.

123 The ozone concentration is determined by the iodometric wet-chemistry method [25].

124 The experiment is carried out at room temperature and atmospheric pressure. The temperature
125 and relative humidity are measured by a TESTO sensor.

126 A schematic diagram of the experimental system is illustrated in Figures 1.a and 1.b.

127

128 **Fig. 1.a: Experimental set-up**

129

130 **Fig. 1.b: General scheme for coupled DBD plasma and photocatalysis**

131

132 **3. Results and discussion**

133

134 The study of ISOVAL removal, the amount of ozone generated and the selectivities of CO
135 and CO₂ was carried out for three reactor configurations (Fig. 1.b): photocatalysis, DBD
136 plasma, and combined DBD plasma/photocatalysis. The influence of some operating
137 parameters on each process performance was investigated. The experiments, which were
138 repeated twice, showed good reproducibility with 5% standard deviation. This is represented
139 by vertical bars in the experimental results in all figures.

140 Before every experiment, the power was turned off (UV and/or electric discharge) and then,
141 once the inlet and outlet concentrations of VOCs were the same (adsorption equilibrium
142 state), the reactor power was turned on. Output samples were collected at 30- to 60-minute
143 intervals until a steady state was achieved. At the end of the experiment, the reactor was
144 cleaned by a flow of clean air for at least one hour.

145

146 **3.1. Effect of Specific Energy (SE)**

147

148 SE is related directly to the energy consumption for the removal of the pollutant. Thus,
149 it can influence the performance of the process.

150 The plasma-injected energy per cycle (E) is determined by the Lissajous plot method [26],
 151 which enables the power input injected (P) as well as the specific energy (SE) to be calculated
 152 as follows:

$$153 \quad P \text{ (W)} = E \text{ (J)} \times \text{frequency (Hz)} \quad (1)$$

$$154 \quad SE \text{ (J/L)} = P \text{ (W)} / Q \text{ (m}^3 \cdot \text{s}^{-1}) / 1000 \quad (2)$$

155 where Q represents the flow rate.

156 The power value (P) is adjusted by changing the applied voltage (U_a).

157

158 3.1.1. On the removal of isovaleraldehyde

159

160 The removal capacity of isovaleraldehyde RC ($\text{mg} \cdot \text{h}^{-1}$) is calculated as:

$$161 \quad RC = Q \cdot \frac{C_{in}}{100} \cdot IRE(\%) \quad (3)$$

162 where IRE(%) isovaleraldehyde conversion is defined as:

$$163 \quad IRE (\%) = \frac{C_{in} - C_{out}}{C_{in}} \times 100 \% \quad (4)$$

164 where C_{in} and C_{out} are the inlet and outlet pollutant concentrations ($\text{mg} \cdot \text{m}^{-3}$), respectively and

165 Q is the flow rate ($\text{m}^3 \cdot \text{h}^{-1}$).

166 Previous experiments have shown the ability of a non-thermal surface plasma discharge to
 167 activate the photocatalyst, such as TiO_2 [27]. In order to investigate the effect of plasma UV
 168 on TiO_2 activity, a study of ISOVAL removal in a DBD plasma reactor in the presence of
 169 photocatalyst was carried out without external UV.

170

171 **Fig. 2: Dependence of SE on ISOVAL removal *in situ* in different plasma systems**
 172 **without external UV.**

173

174 Fig. 2 shows that ISOVAL removal efficiency is not enhanced in the presence of
175 photocatalyst without external UV. Thus, the UV light generated by the DBD reactor is too
176 weak to activate TiO_2 and its contribution to ISOVAL removal can be ignored. This result is
177 in agreement with work on the removal of the ammonia gas [20].

178 In contrast, the introduction of external UV light to the plasma significantly improves the IRE.
179 Fig. 3 shows that when SE increases, the IRE increases as well. For example, with plasma
180 alone, when SE is three times greater, the IRE increases from 44 to 76%. The same behavior
181 is observed when DBD plasma is combined with photocatalysis (Fig. 3). This phenomenon is
182 expected as, by increasing the voltage across the reactor, the electric field in the reactor
183 annulus can be enhanced, resulting in a higher degree of ionization [18, 21-22]. Therefore, the
184 pollutant is more likely to be attacked by electrons or radicals resulting in a greater removal of
185 ISOVAL.

186 When only the photocatalysis process is used, the IRE is about 45%.

187

188 **Fig. 3: Variation of ISOVAL removal efficiency with SE using the three processes (Q
189 $= 2 \text{ m}^3 \cdot \text{h}^{-1}$, $T = 20 \text{ }^\circ\text{C}$, $\text{RH} = 5\%$, $I = 20 \text{ W} \cdot \text{m}^{-2}$).**

190

191 By comparing the IRE (Fig. 3), it is clear that with coupled DBD plasma/photocatalysis and
192 external UV, ISOVAL is easily removed. Moreover, for an inlet concentration of $75 \text{ mg} \cdot \text{m}^{-3}$,
193 Fig. 3 shows that ISOVAL can be completely removed by coupled DBD
194 plasma/photocatalysis when the SE is higher than $17 \text{ J} \cdot \text{L}^{-1}$.

195 In fact, the reactive species generated can efficiently oxidize ISOVAL and thus improve the
196 IRE. Both energetic electrons and atomic oxygen (O^\bullet) are the main reactive species
197 responsible for ISOVAL removal in the air stream. The number of reactive species can be
198 greatly increased in the presence of a photocatalyst, which explains why combined DBD

199 plasma/photocatalysis performs better in terms of ISOVAL abatement than DBD plasma
200 alone.

201

202 3.1.2. On the selectivity of CO and CO₂

203

204 Isovaleraldehyde is mostly converted to CO₂, CO and other organic compounds. The
205 variations of overall CO and CO₂ selectivity are represented in Figure 4. These latter
206 parameters are calculated as follows:

$$207 \quad \{CO_x \text{ selectivity (\%)}\} = \frac{[CO_x]_{isov}^{out} - [CO_x]_{isov}^{in}}{5 \times [ISOVAL]^{in} \times \{\% IRE\}} \times 10^4 \quad (5)$$

208 where $x = 1$ for CO and $x = 2$ for CO₂. $[CO_x]^{in}$ and $[CO_x]^{out}$ are the inlet and outlet
209 concentrations of carbon mono/dioxide respectively (ppmv). $[ISOVAL]^{in}$ is the inlet
210 concentration of ISOVAL (ppmv). The number 5 is the stoichiometric coefficient of the
211 removal reaction.

212 In the first instance, it can be seen (Fig. 4) that CO selectivity can be considered negligible
213 with plasma and coupled DBD plasma/photocatalysis. Certainly, no CO is produced with
214 photocatalysis alone. This result is in agreement with works on the photocatalytic removal of
215 cyclohexane [13], trichloroethylene [11] and formaldehyde [28].

216 Concerning CO₂ selectivity, the increase in SE leads to more mineralization because more
217 electrons and reactive species are produced and thus the ISOVAL byproducts are more
218 mineralized [29]. In fact, when SE increases from 9 to 17 J.L⁻¹, CO₂ selectivity (with DBD
219 plasma alone) increases from 15 to 39%. It is interesting to note that when DBD plasma is
220 coupled to photocatalysis, CO₂ selectivity varies from 40 to 66%. Consequently, this behavior
221 is due to the photocatalytic activity of TiO₂ in the presence of UV radiation. In fact, when the
222 two processes are combined, carbon dioxide selectivity improves compared to DBD plasma

223 alone, whatever the value of SE [26, 30]. Moreover, some intermediates generated by
 224 ISOVAL removal are probably deposited on the photocatalyst surface where mineralization
 225 can thus occur [10]. This result is similar to many studies reported on acetylene [26, 31].
 226 The photocatalysis process is not concerned by SE variation. However, it is interesting to note
 227 that this process leads to the best CO₂ selectivity. Many research works confirm that such
 228 mineralization improvements are related to the porosity of the medium: porosity induces a
 229 longer residence time of gas byproducts during diffusion through the solid pore system [10,
 230 27, 32, 33].

231

232 **Fig. 4: Variation of CO and CO₂ selectivities vs. SE using three processes:**

233 **empty symbol = selectivity of CO and full symbol = selectivity of CO₂**

234 **([ISOVAL] = 75 mg.m⁻³, Q = 2 m³.h⁻¹, T = 20 °C, RH = 5%, I = 20 W.m⁻²).**

235

236 On the other hand, in our study, the byproducts are process-dependent. In fact, with
 237 photocatalysis, the detected byproducts are propionic acid (CH₃CH₂COOH), acetone
 238 (CH₃COCH₃), acetic acid (CH₃COOH) and CO₂.

239

240 To evaluate the validity of the analytical method, i.e. to ensure that the majority of byproducts
 241 are detected, the carbon balance was estimated. It is equal to the ratio of the sum of carbon
 242 byproducts to the isovaleraldehyde removed. Therefore, for combined DBD
 243 plasma/photocatalysis, the carbon balance is simply calculated as the sum of the ratios
 244 (expressed in percentage) of the number of moles of carbon present in the reaction products
 245 relative to their respective moles in the isovaleraldehyde removed.

246 The carbon balance value is expressed as:

247

$$CB(\%) = \frac{\sum C_{measured}}{\sum C_{ISOVAL\ removed}} \times 100\% \quad (6)$$

248 In order to obtain full insight into the intermediates produced in the reaction process, the
249 residence time was varied by varying the gas flow rate.

250 Fig. 5.a shows that the carbon balance is achieved at 90%, which means that all the main
251 organic byproducts are released from the reactor. Certainly, there are some minor byproducts
252 cannot be detected.

253 As can be seen in Fig. 5.a, the byproducts are residence-time-dependent. When this latter
254 parameter increases, more carbon dioxide is formed.

255

256 **Fig. 5.a Variation of carbon balances and selectivity of CO₂ with residence time using**
257 **photocatalysis alone ([ISOVAL] = 100 mg.m⁻³, T = 20 °C, I = 20 W.m⁻², RH = 50%).**

258

259 With combined DBD plasma/photocatalysis, CO appears while with plasma alone, the
260 detected byproducts are CO₂, CO, acetone and acetic acid. Thus, the possible pathway of
261 ISOVAL removal consists of the simultaneous removal of a carboxylic function and creation
262 of an alcohol function [12, 32-34]. This new function is immediately oxidized into a ketone,
263 initiating a new carboxylic function carried on an 'n - 1' carbon molecule. A degradation
264 pathway is proposed from a literature study and checked through experimental investigations
265 [35]. Consequently, the possible pathway of ISOVAL removal is represented in Fig. 5.b.

266

267 **Fig. 5.b: Possible pathway of ISOVAL removal by coupled plasma/photocatalysis with**
268 **external UV.**

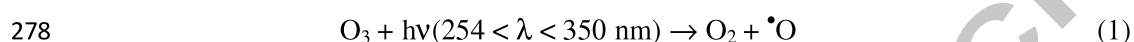
269

270 **3.1.3. On ozone**

271

272 Ozone plays an important role during VOC oxidation. The atomic oxygen formed, due to *in*
273 *situ* decomposition of ozone, interacts with pollutants [36].

274 It can be seen that when SE increases, the quantity of ozone increases too. Moreover, it is
275 interesting to note that the presence of photocatalyst reduces the quantity of ozone in the exit of
276 the reactor. In fact, according to the results of Taranto and co-workers [37], UV radiation can
277 favor ozone destruction by the following reaction [37]:



279 No ozone was found in the exit of our photocatalytic reactor.

280

281 **3.2. Effect of inlet concentration of isovaleraldehyde**

282

283 The second important experimental parameter that can influence process performance is the
284 inlet concentration.

285

286 **3.2.1. On the removal efficiency**

287

288 Fig. 6 illustrates the variation of the IRE versus inlet concentration ranging from 75 to 200
289 $\text{mg}\cdot\text{m}^{-3}$. All experiments were carried out at a constant flow rate ($2 \text{ m}^3\cdot\text{h}^{-1}$), relative humidity
290 (5%) and frequency (50 Hz). The IRE decreases with increasing inlet concentration in all
291 three processes. In the DBD plasma reactor, the IRE falls from 70 to 25% when the inlet
292 concentration increases from 75 to $200 \text{ mg}\cdot\text{m}^{-3}$.

293 Many electrons and reactive species (like $\text{O}\cdot$ and $\text{OH}\cdot$) are needed to remove pollutants from
294 the air stream at a high inlet concentration [21, 26, 30]. With photocatalysis alone, the
295 removal efficiency decreases proportionally with inlet concentration. This is due to the
296 availability of the photocatalytic sites at this concentration range [11, 38, 39].

297

298 **Fig. 6.a: Variation of removal efficiency with inlet concentration using three**
299 **processes (SE = 17 J.L⁻¹, Q = 2 m³.h⁻¹, T = 20 °C, RH = 5%, I = 20 W.m⁻²).**

300

301 Additionally, the synergetic outcome was better demonstrated by comparison of the removal
302 capacities (Table 2), where the RC of the combined system was higher ($\approx 15\%$) than the sum
303 obtained for individually reactors and independent of SE and inlet concentration (100 and 200
304 mg.m⁻³). This indicated that coupling of the photocatalytic and DBD reactors significantly
305 improved removal.

306 The synergetic effect can be ascribed to:

- 307 • several mechanisms occurring when the non-thermal plasma is present since the
308 plasma produces various species such as high-energy electrons, excited molecules or
309 radicals (O[•], N, OH[•], O₂[•], O₃, NO₂, NO_x, etc.). These molecules can interact directly
310 with ISOVAL molecules.
- 311 • plasma promotes the desorption of byproducts attached at the TiO₂ surface and then
312 accelerates the conversion and mineralization [40].
- 313 • plasma can induce activation of TiO₂ by creating a hole/electron pairs by ion
314 bombardment [21, 22, 40].

315

316 **Table.2: RC values for isovaleraldehyde removal by plasma DBD, photocatalysis and a**
317 **coupled process at different inlet concentrations and specific energies.**

318

319 **3.2.2. On the selectivity of CO and CO₂**

320

321 Using photocatalysis alone, when the inlet concentration increases, the selectivity of CO₂
322 decreases (Fig. 7). This means that the quantity of intermediate byproducts generated, except
323 for CO₂, is greater. This behavior is due to the fact that the increase in inlet concentration
324 leads to a lower availability of active sites. Assuming that removal is a series of successive
325 reactions, the competition for the active sites of the catalyst becomes greater when the inlet
326 concentration increases, thus the intermediate byproducts generated cannot be mineralized
327 [7,18, 41, 42].

328 Using DBD plasma alone, the low values of overall CO₂ selectivity are explained by the fact
329 that the quantity of reactive species generated becomes insufficient and the chemical reaction
330 is the limiting step. This result is similar to those in the literature for toluene [43] and benzene
331 [18, 44].

332 On the other hand, combined DBD plasma/photocatalysis enhances CO₂ selectivity
333 significantly, compared to DBD plasma alone. This is attributed to the formation of more
334 reactive species due to the presence of TiO₂ in the plasma discharge zone. Moreover, UV light
335 is able to activate ozone on the surface of TiO₂ in order to improve mineralization.
336 Consequently, possible pathways for pollutant removal in combined DBD
337 plasma/photocatalysis mainly include gas-phase radical attacks due to various other species
338 such as high-energy electrons, excited molecules or radicals (O[•], N, OH[•], O₂[•], O₃, NO₂, NO_x,
339 etc.) [4, 5].

340

341 **Fig. 7: Variation of CO and CO₂ selectivities with inlet concentration using three**
342 **processes: empty symbol represents selectivity of CO and full symbol represents**
343 **selectivity of CO₂ (SE = 17 J.L⁻¹, Q = 2 m³.h⁻¹, T = 20 °C, RH = 5 %, I = 20 W.m⁻²)**

344

345 **3.2.3. On ozone**

346

347 Fig. 8 represents ozone production using the three different processes at different inlet
348 concentrations. With DBD plasma alone, increasing the isovaleraldehyde inlet concentration
349 in the air stream from 75 to 200 mg.m⁻³ halves the amount of ozone. The amount of ozone
350 produced is dependent on ISOVAL concentration. This could be due to the plasma process. A
351 similar trend was observed when using the coupled process.

352

353 **Fig. 8: Variation of amount of ozone with inlet concentration using three processes (SE =**
354 **17 J.L⁻¹, Q = 2 m³.h⁻¹, T = 20 °C, RH = 5%, I = 20 W.m⁻²).**

355

356 3.3. Effect of relative humidity

357

358 The study of the effect of relative humidity (RH) is of great interest since practical
359 applications deal with ambient air that usually contains large amounts of water.

360 In order to understand the influence of RH on the IRE and byproduct formation by DBD
361 plasma and photocatalysis, each oxidative configuration was tested separately: (i)
362 photocatalytic oxidation of ISOVAL (ii) DBD plasma oxidation of ISOVAL and (iii) DBD
363 plasma/photocatalysis combination.

364

365 3.3.1. On isovaleraldehyde removal

366

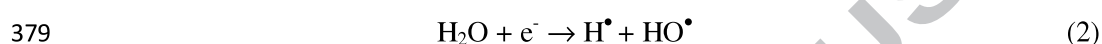
367 Using photocatalysis alone, it is well known that the presence of water molecules in the air
368 stream leads to the formation of OH• radicals [28, 39] which improve the IRE.

369 Here, the IRE increases and then drops. In fact, when RH increases, the competitive effect
370 towards the active sites of water becomes predominant and thus the IRE decreases. In our

371 case, an optimum RH value around 50% is seen (Fig. 9). Many other VOCs like
372 trichloroethylene [45] and cyclohexane [13] show the same behavior toward RH.

373 Nevertheless, when DBD plasma is used, the influence of water vapor on the IRE is not
374 significant (Fig. 9), regardless of the value of SE. The IRE is around 40% whatever the value
375 of RH at SE equal to 17 J.L⁻¹.

376 With combined DBD plasma/photocatalysis, the IRE increases significantly with increasing
377 RH content up to 60%. Certainly, water vapor content enhances the formation of reactive
378 species as in the equation [45-46]:



380 On the other hand, at higher levels of RH, an inverted trend occurs and the IRE becomes
381 slightly lower. This is because the increased water vapor content limits the electron density
382 and quenches the active chemical species [4, 5]. This behavior is similar to that reported in the
383 literature for some VOCs [44-46].

384

385 **Fig. 9: Variation of IRE vs. RH using three processes ([ISOVAL]₀ = 100 mg.m⁻³, Q = 2**
386 **m³.h⁻¹, T = 20 °C, SE = 17 J.L⁻¹, I = 20 W.m⁻²).**

387

388 Moreover, as shown in Table 3 the variation of RH does not affect the synergistic effect in
389 combined DBD plasma/photocatalysis. In fact, at each value of RH, the RC due to the
390 combined process is higher than the value corresponding to the sum of the removal capacities
391 of each process taken separately.

392

393 **Table.3: RC values for isovaleraldehyde removal by plasma DBD, photocatalysis and a**
394 **coupled process at different RH.**

395

396 3.3.2. On the selectivities of CO and CO₂

397

398 As shown on Fig. 10, water vapor has a significant effect on CO₂ selectivity. In fact, when RH
399 increases from 5 to 90%, with DBD plasma alone, CO₂ selectivity increases from 31 to 48%.

400 As previously described, a small amount of water vapor is essential for the formation of active
401 species (such as OH[•] and O[•]) which leads to more mineralization of byproducts. Additionally,
402 it is interesting to note that there is no CO when RH is equal to 90%.

403 With photocatalysis alone, when RH increases from 5 to 60%, CO₂ selectivity remains stable.
404 However, a further increase in RH reduces mineralization. This behavior arises because water
405 vapor can deposit on the surface of the photocatalyst and occupy its active sites. If the number
406 of active sites is considered constant, it becomes evident that the competitive effect increases
407 with increasing RH.

408 With coupled plasma DBD plasma/photocatalysis, CO₂ selectivity increases by about 20%
409 compared to DBD plasma alone (Fig. 10). For the above reason, it might be concluded that
410 the photocatalyst leads to more ISOVAL mineralization because the presence of OH[•] radicals
411 greatly improves the oxidation of CO into CO₂ [48]. This result is similar to that found in the
412 literature for acetylene [48]. In fact, several authors [48] have reported that CO and CO₂ are
413 related by an equilibrium reaction under plasma action. Moreover, Futamura et al. [49] take
414 this equilibrium between CO and CO₂ into account and suggest that the presence of OH[•]
415 radicals shifts the equilibrium towards the formation of CO₂.

416

417 **Fig. 10: Variation of the overall selectivity of CO₂ vs. RH**

418 ([ISOVAL] = 100 mg.m⁻³, Q = 2 m³.h⁻¹, T = 20 °C, SE = 17 J.L⁻¹, I = 20 W.m⁻²).

419

420 3. 3. 3. On ozone

421

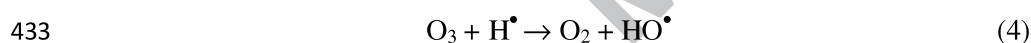
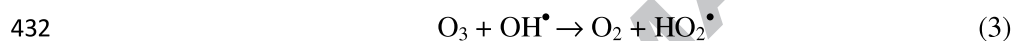
422 The results of ozone production at different RH are reported in Fig. 11. With DBD plasma
 423 alone, ozone is strongly reduced when RH increases (Fig. 11). Its formation is probably
 424 inhibited. For example, the quantity of ozone is reduced three times when RH increases from
 425 30 to 60-65%.

426

427 **Fig. 11: Variation of the amount of ozone with RH using three processes ($[\text{ISOVAL}]_0 =$
 428 100 mg.m^{-3} , $Q = 2 \text{ m}^3.\text{h}^{-1}$, $T = 20 \text{ }^\circ\text{C}$, $SE = 17 \text{ J.L}^{-1}$, $I = 20 \text{ W.m}^{-2}$).**

429

430 The consumption of ozone in the presence of radicals ($\text{H}^\bullet + \text{HO}^\bullet$) can be explained by these
 431 two reactions [50, 51]:



434 Similar trends were observed for coupled DBD plasma/photocatalysis.

435

436 Conclusion

437

438 Many parameters were investigated in this work such as SE, inlet concentration of
 439 isovaleraldehyde and RH. Their influences on the performances of three processes (DBD
 440 plasma, photocatalysis and combined DBD plasma/photocatalysis) were studied.

441 An increase in inlet concentration greatly modifies the oxidative processes: (i) the IRE is
 442 considerably slowed down; (ii) the mineralization of ISOVAL is reduced. However,
 443 increasing SE improves both the IRE and mineralization of ISOVAL.

444 Water vapor plays a very important role in the elimination of ISOVAL. An optimum RH
 445 value is observed with photocatalysis alone and with the combined process. Water vapor also

446 improves CO₂ selectivity and decreases the amount of CO. On the other hand, RH reduces
447 ozone formation.

448 For each operating parameter, we have shown unambiguously that a synergetic effect on
449 ISOVAL removal can be observed when DBD plasma is coupled with TiO₂ catalyst irradiated
450 by external UV.

451 Moreover, the byproducts of DBD plasma, photocatalysis and combined DBD
452 plasma/photocatalysis have been identified and evaluated. A possible pathway for ISOVAL
453 removal is proposed.

454

455 Acknowledgments

456

457 The authors wish to thank the French National Research Agency (ANR) for supporting this
458 research. They also thank the Ahlstrom Company for providing the photocatalytic medium.

459

460

461

462

463

464

465

466

467

468

469

470

471 **References**

- 472 [1] B. Eliasson, W. Egli and U. Kogelschatz, Modelling of dielectric barrier discharge chemistry, Pure & Appl.
473 Chsm., 66 (1994) 1275-1286.
- 474
- 475 [2] ADEME, 2005. Pollutions olfactives : origine, législation, analyse, traitement, Ademe, Dunod, Angers.
476
- 477 [3] P. Le Cloirec, 1998. Les composés organiques volatils (COV) dans l'environnement, Lavoisier, Tec&Doc,
478 Paris.
- 479
- 480 [4] H. Huang, D. Ye, D. Y. C. Leung, Plasma-driven catalysis process for toluene abatement: effect of water
481 vapor, IEEE Transactions on Plasma Science, 39 (2011) 576 – 580.
- 482
- 483 [5] H. Huang, D. Yea, D. Y. C. Leung, F. Feng, X. Guan, Byproducts and pathways of toluene destruction via
484 plasma-catalysis, Journal of Molecular Catalysis A: Chemical 336 (2011) 87–93.
- 485
- 486 [6] P. Monneyron, M. H. Manéro, S. Mathe, A combined selective adsorption and ozonation process for VOCs
487 removal from air, The Canadian Journal of Chemical Engineering 85 (2007) 326-332.
- 488
- 489 [7] T. Ochiai, T. Hoshi, H. Slimen, K. Nakata, T. Murakami, H. Tatejima, Y. Koide, A. Houas, T. Horie, Y.
490 Morito, A. Fujishima, Fabrication of TiO₂ nanoparticles impregnated titanium mesh filter and its application for
491 environmental purification unit, Catal. Sci. Technol. 1 (2011) 1324–1327
- 492
- 493 [8] T. Ochiai, K. Nakata, T. Murakami, T. Horie, Y. Morito, A. Fujishima, Anodizing effects of titanium-mesh
494 surface for fabrication of photocatalytic air purification filter, Nanosci. Nanotechnol. Lett. 4 (2012) 544–547.
- 495
- 496 [9] S. Yao, E. Suzuki and A. Nakayama, a novel pulsed plasma for chemical conversion. Thin Solid Films, 390
497 (2001) 165-169.
- 498
- 499 [10] S. Futamura, H. Kabashima and G. Annadurai, Roles of CO₂ and H₂O as oxidants in the plasma reforming
500 of aliphatic hydrocarbons. Catalysis Today 115 (2006) 211–216.

501

502 [11] R. Ben Gadri, J. R. Roth, T. C. Montie, K. Kelly-Wintenber, P P.-Y. Tsai, D. J. Helfritch, P. Feldman, D. M.
503 Sherman, F. Karakaya, Zh.u Chen, Sterilization and plasma processing of room temperature surfaces with a one
504 atmosphere uniform glow discharge plasma OAugDP Surface and Coatings Technology 131 (2000) 528-542.

505

506 [12] H. H. Kim, K. Takashima, S. Katsura , A. Mizuno,, Low-temperature NOx reduction processes using
507 combined systems of pulsed corona discharge and catalysts, J. Phys. D : Appl. Phys., 34 (2001) 604-613.

508 [13] Y. S. Mokt, H. W. Lee, Y. J. Hyun, S. W. Ham, I.-S. Nam, Determination of Decomposition Rate Constants
509 of Volatile Organic Compounds and Nitric Oxide in a Pulsed Corona Discharge Reactor, Korean J. Chem. Eng,
510 18 (2001) 711-718.

511

512 [14] M. Derakhshesh, J. Abedi, H. Hassanzadeh, Mechanism of methanol decomposition by non-thermal plasma,
513 Journal of Electrostatics 68 (2010) 424-428.

514

515 [15] S. Delagrange, L. Pinard, J.-M. Tatibouet, Combination of a non-thermal plasma and a catalyst for toluene
516 removal from air: Manganese based oxide catalysts, Applied Catalysis B: Environmental 68, (2006) 92–98.

517 [16] A. A. Assadi, A. Bouzaza, M. Lemasle, D. Wolbert, Removal of trimethylamine and isovaleric acid from
518 gas streams in a continuous flow surface discharge plasma reactor, Chemical Engineering Research and Design,
519 in press.

520

521 [17] K. Allegraud, Décharge à Barrière Diélectrique de Surface : physique et procédé, thèse Ecole polytechnique
522 de Paris, 2008.

523

524 [18] H.M. Lee, M.B. Chang, Gas-phase removal of acetaldehyde via packed-bed dielectric barrier discharge
525 reactor, Plasma Chem. Plasma Process. 21(2001) 329-343.

526 [19] Ch. Subrahmanyama, A. Renken, L. Kiwi-Minsker, Catalytic non-thermal plasma reactor for abatement of
527 toluene, Chemical Engineering Journal, 160 (2010) 677–682.

528

529 [20] T. Ochiai, K. Nakata, T. Murakami, Y. Morito, S. Hosokawa, A. Fujishima, Development of an air-
530 purification unit using a photocatalysis-plasma hybrid reactor, Electrochemistry 79 (2011) 838–841

531

532 [21] J. Chen, Zh. Xie, Removal of H₂S in a novel dielectric barrier discharge reactor with photocatalytic
533 electrode and activated carbon fiber, *Journal of Hazardous Materials* 261 (2013) 38–43

534

535 [22] T. Ochiai, Y. Hayashi, M. Ito, K. Nakata, T. Murakami, Y. Morito, A. Fujishima, An effective method for a
536 separation of smoking area by using novel photocatalysis-plasma synergistic air-cleaner, *Chemical Engineering*
537 *Journal* 209 (2012) 313–317.

538

539 [23] Ahlstrom Patent EP 1069950, 2000. AU 735798 US 09/467, 650; JP 2000-542104.

540

541 [24] CIAT Patent, Dispositif, système et procédé de traitement de gaz, 2013, EP 1000180221,
542 BFF11L1041/MFH.

543

544 [25] R. Atkinson, D. L. Baulch, R. A. Cox, J. N. Crowley, R. F. Hampson, R. G. Hynes, M. E. Jenkin, M. J.
545 Rossi, J. Troe. Evaluated kinetic and photochemical data for atmospheric chemistry: Part 1 - gas phase reactions
546 of Ox, HOx, NOx and Sox species. *Atmospheric Chemistry and Physics Discussions*, 3 (2003) 6179–6699.

547

548 [26] T. C. Manley, 1943. *Proceedings of the 84th General Meeting*, New York.

549

550 [27] O. Guaitella, F. Thevenet, E. Puzenat, C. Guillard, A. Rousseau, C₂H₂ oxidation by plasma/TiO₂
551 combination: Influence of the porosity, and photocatalytic mechanisms under plasma exposure, *Applied*
552 *Catalysis B: Environmental*, 80 (2008) 296–305.

553

554 [28] T. N. Obee, R. T. Brown, TiO₂ photocatalysis for indoor air applications: effects of humidity and trace
555 contaminant levels on the oxidation rates of formaldehyde, toluene, and 1, 3-butadiene, *Environmental Science*
556 *and Technology*. 29 (1995)1223-1231.

557

558 [29] A. M. Vandenbroucke, R. Morent, , N. De Geyter, Ch. Leys, Non-thermal plasmas for non-catalytic and
559 catalytic VOC abatement, *Journal of Hazardous Materials* 195 (2011) 30–54.

560

- 561 [30] O. Guaitella, C. Lazzaroni, D. Marinov, A. Rousseau, Evidence of atomic adsorption on TiO₂ under plasma
562 exposure and related C₂H₂ surface reactivity, *Applied Physics Letters*, 97 (2010) 011502 (0) - 011502 (3)
563
- 564 [31] H. B. Huang, D. Q. Ye, M. L. Fu, F. D. Feng., contribution of UV light to the decomposition of toluene in
565 dielectric barrier discharge plasma/photocatalysis system, *Plasma Chem. Plasma Process* 27 (2007) 577–588.
566
- 567 [32] A. A. Assadi, A. Bouzaza, D. Wolbert, P. Petit, Isovaleraldehyde elimination by UV/TiO₂ photocatalysis:
568 comparative study of the process at different reactors configurations and scales, *Environmental Science and*
569 *Pollution Research* in press.
- 570 [33] D. D. Dionysiou, M. T. Suidan, I. Baudin, J.-M. Lainé, Oxidation of organic contaminants in a rotating disk
571 photocatalytic reactor: reaction kinetics in the liquid phase and the role of mass transfer based on the
572 dimensionless Damköhler number, *Applied Catalysis B: Environmental* 38 (2002) 1–16.
573
- 574 [34] A. A. Assadi, J. Palau, Bouzaza A., D. Wolbert, A continuous air reactor for photocatalytic degradation of
575 Isovaleraldehyde: Effect of different operating parameters and chemical degradation pathway. *Chemical*
576 *Engineering Research and Design* 91 (2013) 1307–1316
577
- 578 [35] B. Boulinguez, A. Bouzaza, S. Merabet, D. Wolbert. Photocatalytic degradation of ammonia and butyric
579 acid in plug-flow reactor: Degradation kinetic modeling with contribution of mass transfer, *Journal of Chemistry*
580 *and Photobiology A: Chemistry* 200 (2008) 254–261.
581
- 582 [36] H. Wang, D. Li, Y. Wu, J. Li, L. Guofeng, Removal of four kinds of volatile organic compounds mixture in
583 air using silent discharge reactor driven by bipolar pulsed power, *Journal of Electrostatics* 67 (2009) 547–555.
584
- 585 [37] J. Taranto, D. Frochot, P. Pichat, Combining Cold Plasma and TiO₂ Photocatalysis To Purify Gaseous
586 Effluents: A Preliminary Study Using Methanol-Contaminated Air, *Ind. Eng. Chem. Res.* 46 (2007) 7611-7614.
587
- 588 [38] A. Queffeuilou, L. Geron, E. Schaer, Prediction of photocatalytic air purifier apparatus performances with a
589 CFD approach using experimentally determined kinetic parameters, *Chemical Engineering Science.* 65 (2010)
590 5067–5074.

591

592 [39] T. Ochiai, A. Fujishima, Photoelectrochemical properties of TiO₂ photocatalyst and its applications for
593 environmental purification, *Journal of Photochemistry and Photobiology C: Photochemistry Reviews* 13 (2012)
594 247–262.

595

596 [40] L. Sivachandiran, F. Thevenet, A. Rousseau, Non-Thermal Plasma Assisted Regeneration of Acetone
597 Adsorbed TiO₂ Surface, *Plasma Chem. Plasma Process* 33 (2013) 855–871.

598

599 [41] Ch.-L. Chang, T.-Sh. Lin, Decomposition of Toluene and Acetone in Packed Dielectric Barrier discharge
600 Reactor, *Plasma Chemistry and Plasma Processing*, 25 (2005) 227-243.

601

602 [42] N. Harada, T. Matsuyama, H. Yamamot, Decomposition of volatile organic compounds by a novel electrode
603 system integrating ceramic filter and SPCP method, *Journal of Electrostatics*, 65 (2007) 43–53.

604

605 [43] D. Li, D. Yakushiji, S. Kanazawa, T. Ohkubo, Y. Nomoto, Decomposition of toluene by streamer corona
606 discharge with catalyst, *J. Electrostat.*, 55 (2002) 311-319.

607

608 [44] B. Y. Lee, S. H. Park, S.C. Lee, M. Kang, S.-J. Choung, Decomposition of benzene by using a discharge
609 plasma–photocatalyst hybrid system, *Catal. Today*, 93 (2004) 769-776.

610 [45] K. H. Wang, H. H. Tsai, Y. H. Hsieh, The kinetics of photocatalytic degradation of trichloroethylene in gas
611 phase over TiO₂ supported on glass bead, *Appl. Catal. B: Environ.* 17 (1998) 313–320.

612

613 [46] Y. Guo, X. Liao, D. Ye, Detection of hydroxyl radical in plasma reaction on toluene removal *Journal of*
614 *Environmental Sciences*, 20 (2008) 1429–1432.

615

616 [47] Z. Bo, J. H. Yan, X. D. Li, Y. Chi, K. F. Cen, B. G. Cheron, Effects of oxygen and water vapor on volatile
617 organic compounds decomposition using gliding arc gas discharge, *Plasma Chem. Plasma Process.*, 275 (2007)
618 546–558,

619

620 [48] F. Thevenet, O. Guaitella, E. Puzenat, C. Guillard, A. Rousseau, 2008. Influence of water vapour on
621 plasma/photocatalytic oxidation efficiency of acetylene, Applied Catalysis B: Environmental, 84 (2008) 813–
622 820.

623

624 [49] J. Chen, Effect of relative humidity on electron distribution and ozone production by DC coronas in air,
625 IEEE transactions on plasma science, 33 (2005) 808-812.

626

627 [50] S. Futamura, A. H. Zhang, T. Yamamoto, The dependence of nonthermal plasma behavior of VOCs on their
628 chemical structures Journal of Electrostatics, 42 (1997) 51-62

629

630

631

632

633

634

635

636

637

638

639

640

641

642

643

644

645

646

647

648

649

650

651 **Table:**

652

653 Table 1: Analysis conditions for the gas chromatograph

654

655 Table 2: RC values ($\text{mg}\cdot\text{h}^{-1}$) for isovaleraldehyde removal by DBD plasma, photocatalysis and656 a coupled process at different inlet concentrations and specific energies ($Q = 2 \text{ m}^3\cdot\text{h}^{-1}$, $T = 20$ 657 $^{\circ}\text{C}$, $\text{RH} = 5\%$, $I = 20 \text{ W}\cdot\text{m}^{-2}$).

658

659 Table 3: RC values ($\text{mg}\cdot\text{h}^{-1}$) for isovaleraldehyde removal by DBD plasma, photocatalysis and660 a coupled process at different relative humidity ($Q = 2 \text{ m}^3\cdot\text{h}^{-1}$, $T = 20 \text{ }^{\circ}\text{C}$, $I = 20 \text{ W}\cdot\text{m}^{-2}$).

661

662

663

664

665

666

667

668

669

670

671

672

673

674

675

676

677

678

679

680

681

682

683

684

685

686

687

688
689
690
691
692
693
694

Gas pressure			Zone temperature	
N ₂ (gas carrier, kPa)	H ₂ (kPa)	Air (kPa)	Injector (°C)	Oven (°C)
105	40	100	110	50

695
696
697
698
699
700
701
702
703
704
705
706
707
708
709
710
711
712
713
714
715
716
717
718
719
720
721
722
723
724
725
726

Table 1: Analysis conditions for the gas chromatograph

727
728
729
730
731

	Inlet concentration	100 mg.m ⁻³	200 mg.m ⁻³
	Photocatalysis	59.80	84.00
SE= 5J/L	DBD plasma	37.87	37.60
	Coupled process	126.6	180.05
SE= 9J/L	DBD plasma	58.00	59.02
	Coupled process	133.2	223.60
SE= 11J/L	DBD plasma	64.39	76.48
	Coupled process	143.8	261.61
SE=17J/L	DBD plasma	79.80	93.20
	Coupled process	171.8	309.43

732
733
734
735
736
737
738
739
740
741
742
743
744
745
746

Table 2: RC values (mg.h⁻¹) for isovaleraldehyde removal by DBD plasma, photocatalysis and a coupled process at different inlet concentrations and specific energies (Q = 2 m³.h⁻¹, T = 20 °C, RH = 5%, I = 20 W.m⁻²)

747
748
749
750
751
752

	Specific energy	SE=9J.L ⁻¹	SE=17J.L ⁻¹
RH= 25%	Photocatalysis	63.04	
	DBD plasma	73.47	82.00
	Coupled process	133.8	178.80
RH=60%	Photocatalysis	70.04	
	DBD plasma	64.00	85.02
	Coupled process	148.68	189.20
RH=90%	Photocatalysis	58.10	
	DBD plasma	56.05	71.60
	Coupled process	130.40	158.08

753
754
755
756
757
758
759
760
761
762
763
764
765
766
767
768
769
770
771

Table 3: RC values (mg.h⁻¹) for isovaleraldehyde removal by DBD plasma, photocatalysis and a coupled process at different relative humidity (Q = 2 m³.h⁻¹, T = 20 °C, I = 20 W.m⁻²)

772 **Figures:**

773

774 Fig. 1.a: Experimental set-up.

775

776 Fig. 1.b: General scheme for coupled non-thermal plasma and photocatalysis.

777

778 Fig. 2: Dependence of SE on ISOVAL removal *in situ* in different plasma systems without external
779 UV.

780

781 Fig. 3: Variation of ISOVAL removal efficiency with SE using the three processes ($Q = 2 \text{ m}^3 \cdot \text{h}^{-1}$, $T =$
782 $20 \text{ }^\circ\text{C}$, $\text{RH} = 5\%$, $I = 20 \text{ W} \cdot \text{m}^{-2}$).

783

784 Fig. 4: Variation of CO and CO₂ selectivities vs. specific energy using three processes: empty symbol
785 = selectivity of CO and full symbol = selectivity of CO₂ ([ISOVAL] = $75 \text{ mg} \cdot \text{m}^{-3}$, $Q = 2 \text{ m}^3 \cdot \text{h}^{-1}$, $T = 20$
786 $^\circ\text{C}$, $\text{RH} = 5\%$, $I = 20 \text{ W} \cdot \text{m}^{-2}$).

787

788 Fig. 5.a: Variation of carbon balances and selectivity of CO₂ with residence time using photocatalysis
789 alone ([ISOVAL] = $100 \text{ mg} \cdot \text{m}^{-3}$, $T = 20 \text{ }^\circ\text{C}$, $I = 20 \text{ W} \cdot \text{m}^{-2}$, $\text{RH} = 50\%$).

790

791 Fig. 5.b: Possible pathway of ISOVAL removal by coupled DBD plasma/photocatalysis with external
792 UV.

793

794 Fig. 6: Variation of removal efficiency with inlet concentration using three processes ($\text{SE} = 17 \text{ J} \cdot \text{L}^{-1}$, Q
795 $= 2 \text{ m}^3 \cdot \text{h}^{-1}$, $T = 20 \text{ }^\circ\text{C}$, $\text{RH} = 5\%$, $I = 20 \text{ W} \cdot \text{m}^{-2}$).

796

797 Fig. 7: Variation of CO and CO₂ selectivities with inlet concentration using three processes: empty
798 symbol represents selectivity of CO and full symbol represents selectivity of CO₂ (SE = 17 J.L⁻¹, Q = 2
799 m³.h⁻¹, T = 20 °C, RH = 5%, I = 20 W.m⁻²).

800

801 Fig. 8: Variation of the amount of ozone with inlet concentration using three processes (SE = 17 J.L⁻¹,
802 Q = 2 m³.h⁻¹, T = 20 °C, RH = 5%, I = 20 W.m⁻²).

803

804 Fig. 9: Variation of isovaleraldehyde removal efficiency vs. RH using three processes ([ISOVAL]₀ =
805 100 mg.m⁻³, Q = 2 m³.h⁻¹, T = 20 °C, SE = 17 J.L⁻¹, I = 20 W.m⁻²).

806

807 Fig. 10: Variation of the overall selectivity of CO₂ vs. RH ([ISOVAL] = 100 mg.m⁻³, Q = 2 m³.h⁻¹, T =
808 20 °C, SE = 17 J.L⁻¹, I = 20 W.m⁻²).

809

810 Fig. 11: Variation of the amount of ozone with relative humidity using three processes ([ISOVAL]₀ =
811 100 mg.m⁻³, Q = 2 m³.h⁻¹, T = 20 °C, SE = 17 J.L⁻¹, I = 20 W.m⁻²).

812

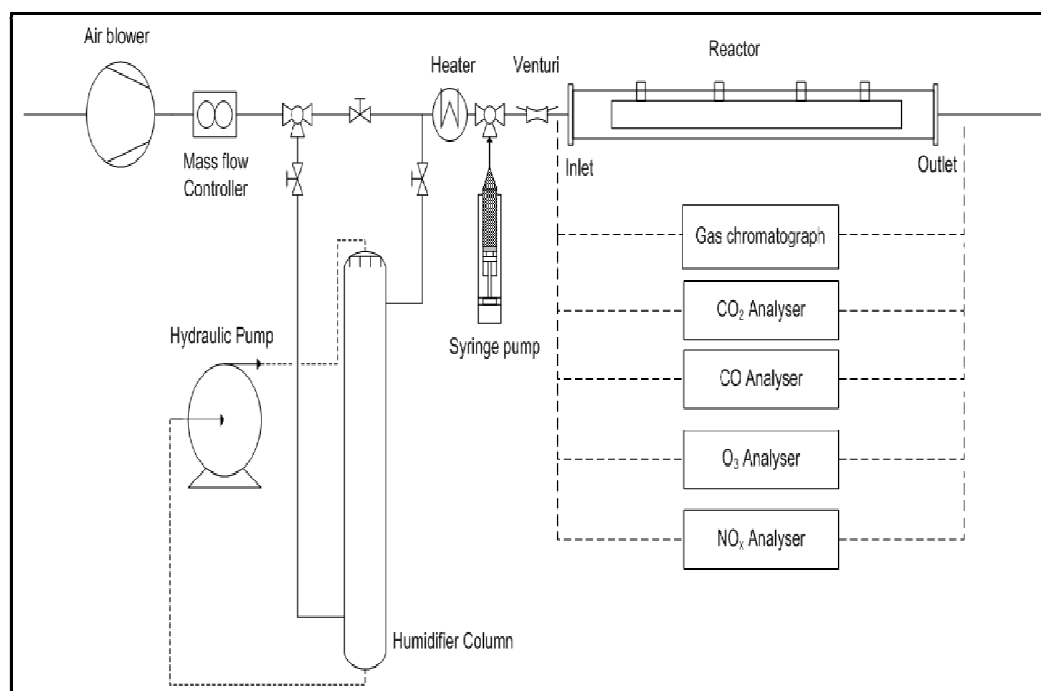
813

814

815

816

817



818

819

Fig. 1.a: Experimental set-up.

820

821

822

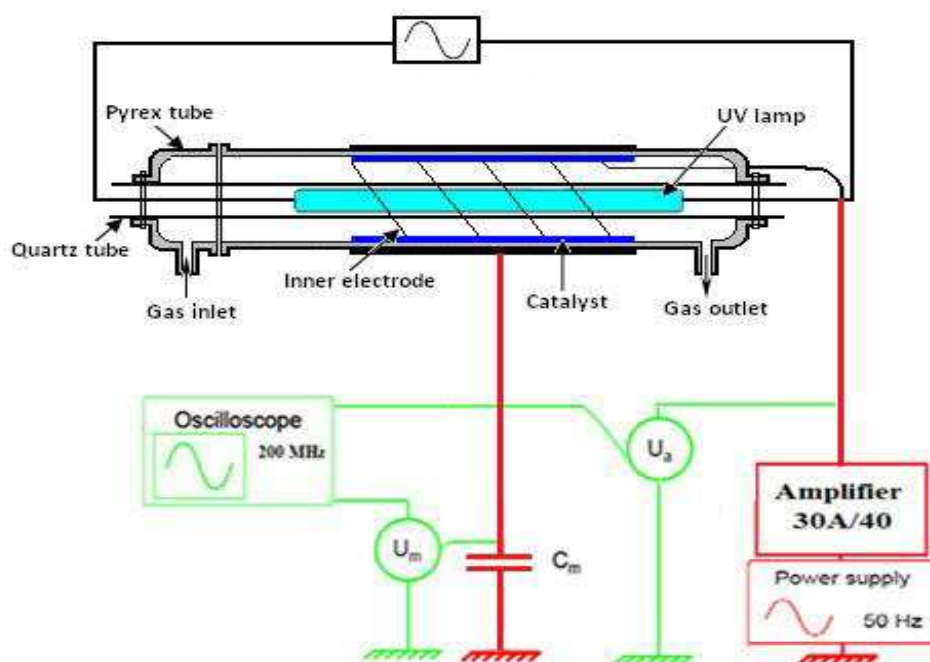
823

824

825

826

827



828

829

830 Fig. 1.b: General scheme for coupled non-thermal plasma and photocatalysis.

831

832

833

834

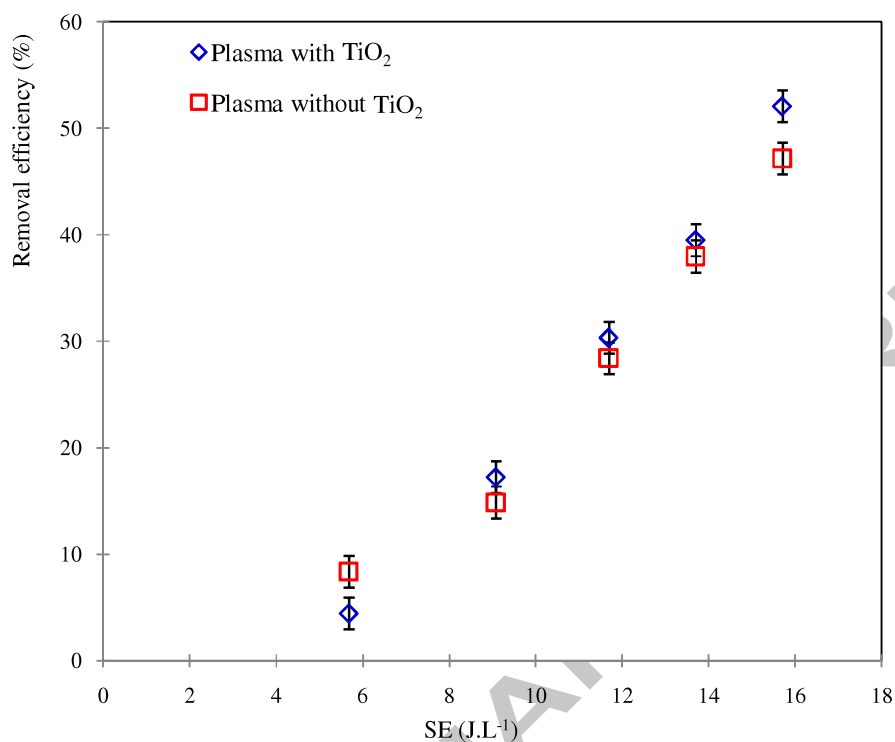
835

836

837

838

839



840

841 Fig. 2: Dependence of SE on ISOVAL removal *in situ* in different plasma systems without
842 external UV ([ISOVAL] = 100 mg.m⁻³, Q = 1 m³.h⁻¹, T = 20 °C, RH = 5%, I = 20 W.m⁻²).

843

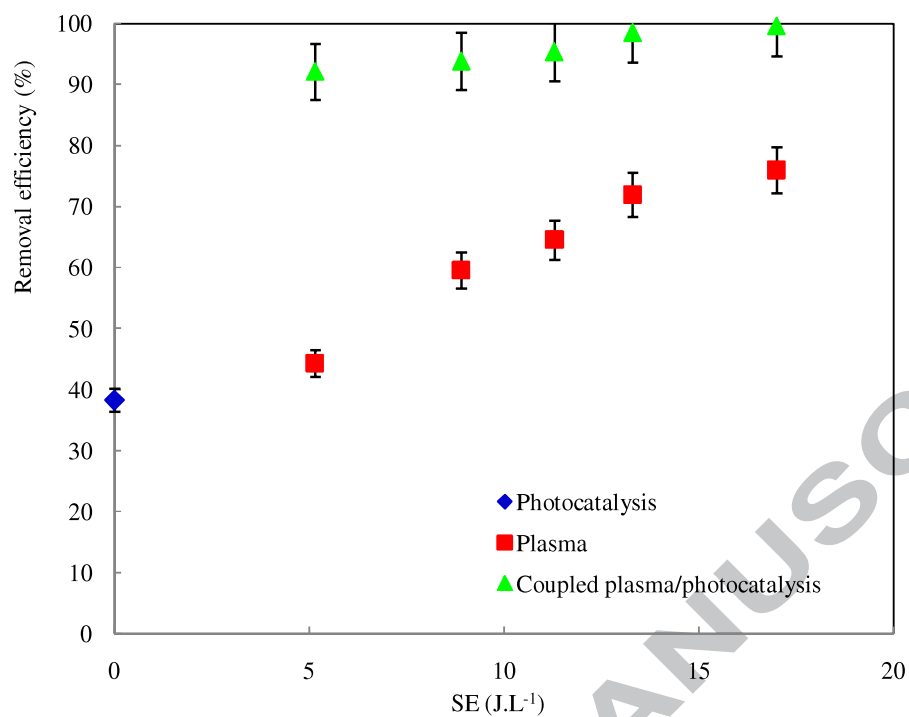
844

845

846

847

848



849

850 Fig. 3: Variation of ISOVAL removal efficiency with SE using the three processes

851 ([ISOVAL] = 75 mg.m⁻³, Q = 2 m³.h⁻¹, T = 20 °C, RH = 5%, I = 20 W.m⁻²).

852

853

854

855

856

857

858

859

860

861

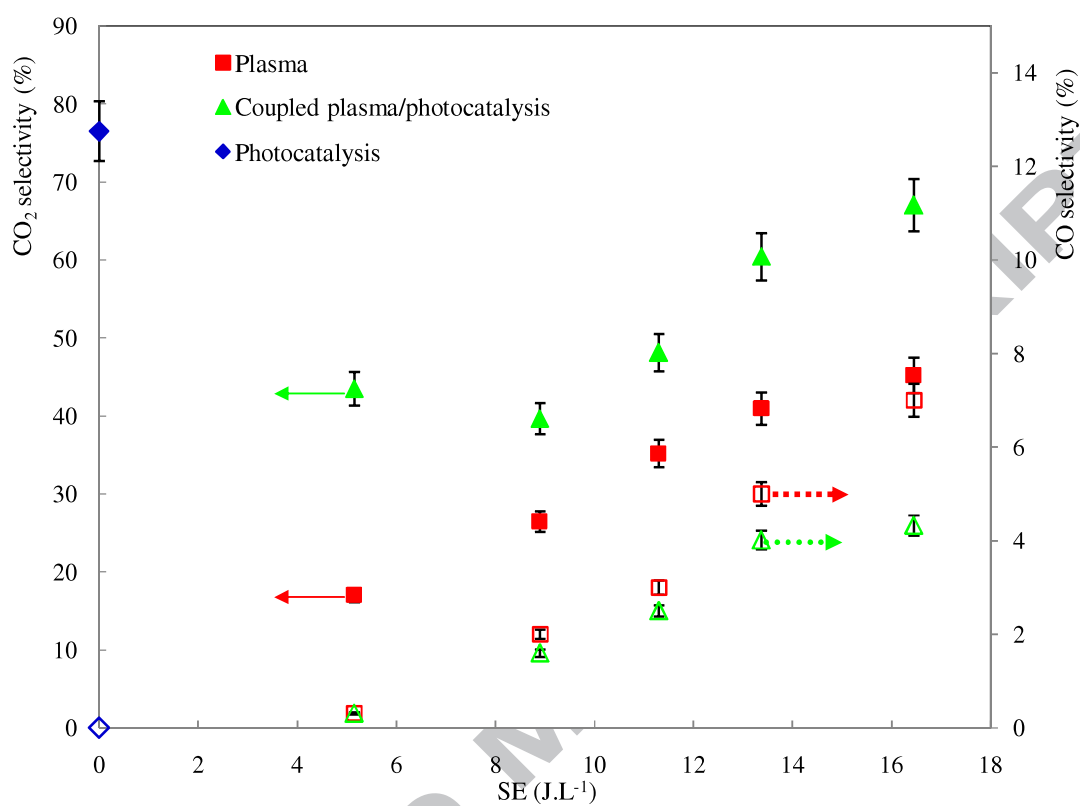
862

863

864

865

866



867

868

869 Fig. 4: Variation of CO and CO₂ selectivities vs. SE using three processes:870 empty symbol = selectivity of CO and full symbol = selectivity of CO₂871 ([ISOVAL] = 75 mg.m⁻³, Q = 2 m³.h⁻¹, T = 20 °C, RH = 5%, I = 20 W.m⁻²).

872

873

874

875

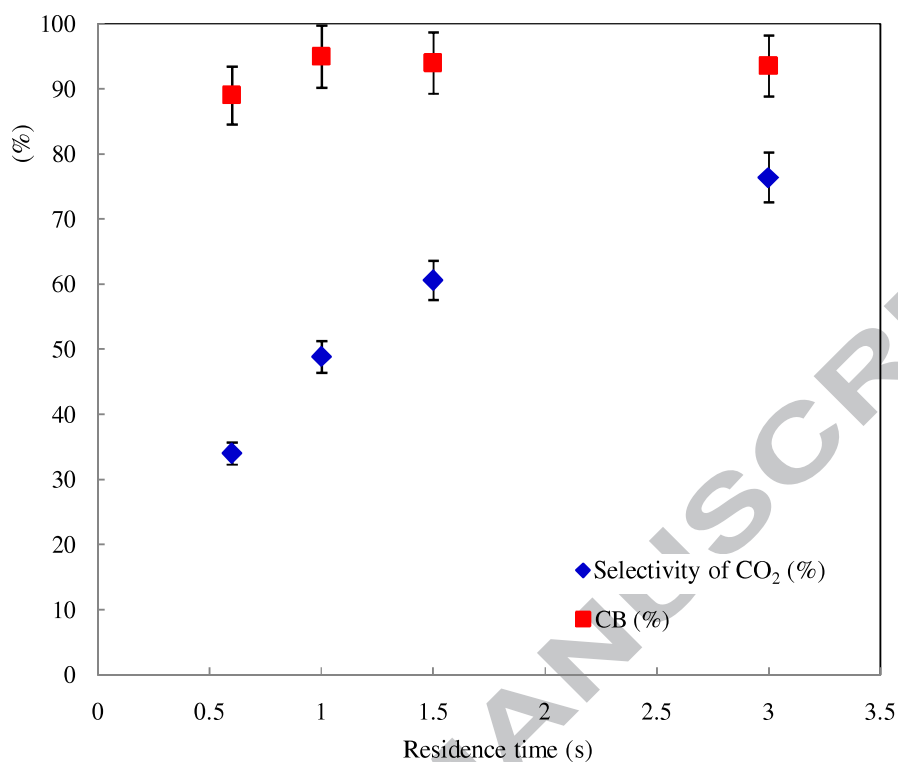
876

877

878

879

880



881

882 Fig. 5.a: Variation of carbon balances and selectivity of CO₂ with residence time using
883 photocatalysis alone ([ISOVAL] = 75 mg.m⁻³, T = 20 °C, I = 20 W.m⁻², RH = 5%).

884

885

886

887

888

889

890

891

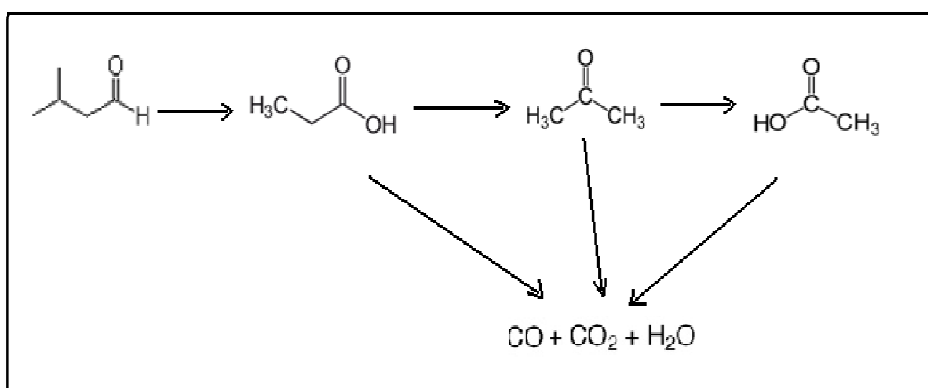
892

893

894

895

896



897

898 Fig. 5.b: Possible pathway of ISOVAL removal by coupled DBD plasma/photocatalysis.

899

900

901

902

903

904

905

906

907

908

909

910

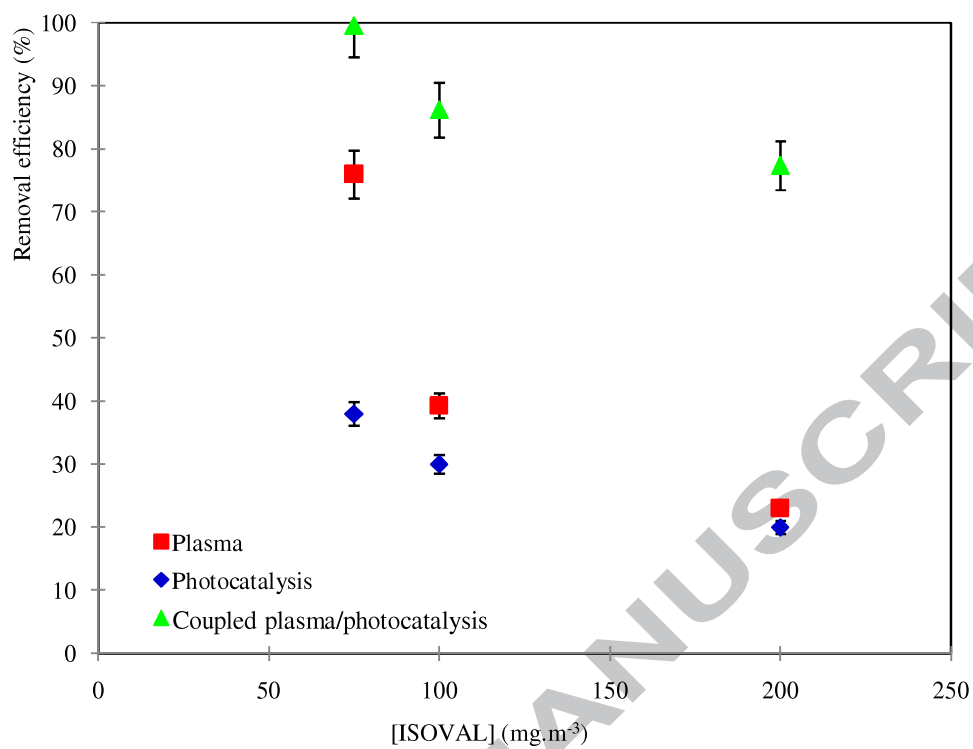
911

912

913

914

915



916

917 Fig. 6: Variation of removal efficiency with inlet concentration using three processes (SE =

918

17 J.L⁻¹, Q = 2 m³.h⁻¹, T = 20 °C, RH = 5%, I = 20 W.m⁻²).

919

920

921

922

923

924

925

926

927

928

929

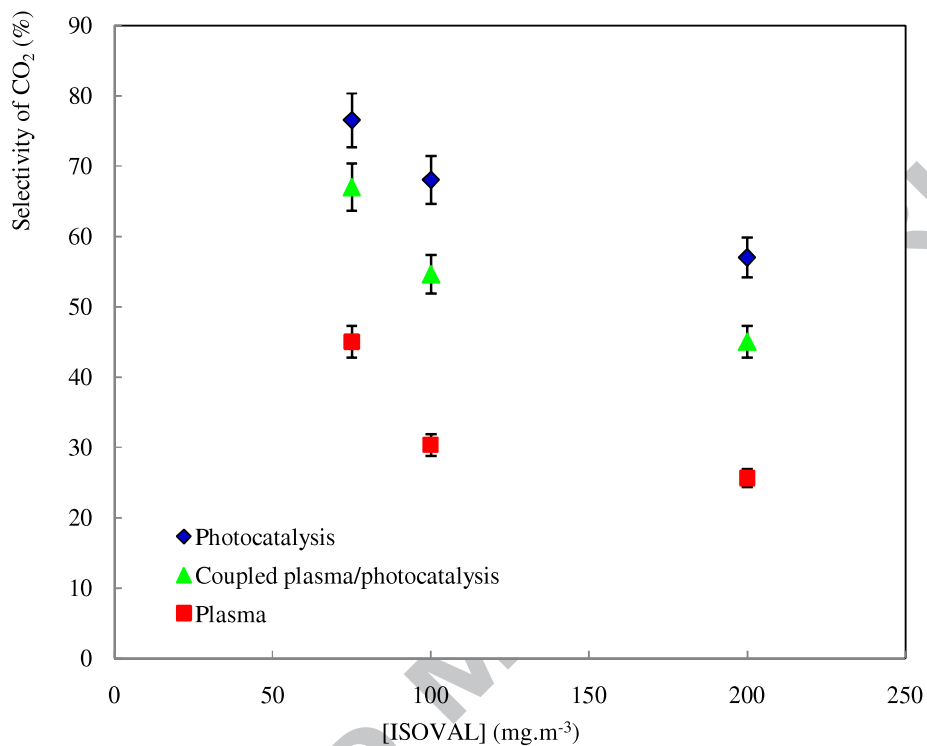
930

931

932

933

934



935

936 Fig. 7: Variation of CO₂ selectivities with inlet concentration using three processes: (SE = 17

937

 J.L^{-1} , $Q = 2 \text{ m}^3 \cdot \text{h}^{-1}$, $T = 20 \text{ }^\circ\text{C}$, $\text{RH} = 5\%$, $I = 20 \text{ W.m}^{-2}$).

938

939

940

941

942

943

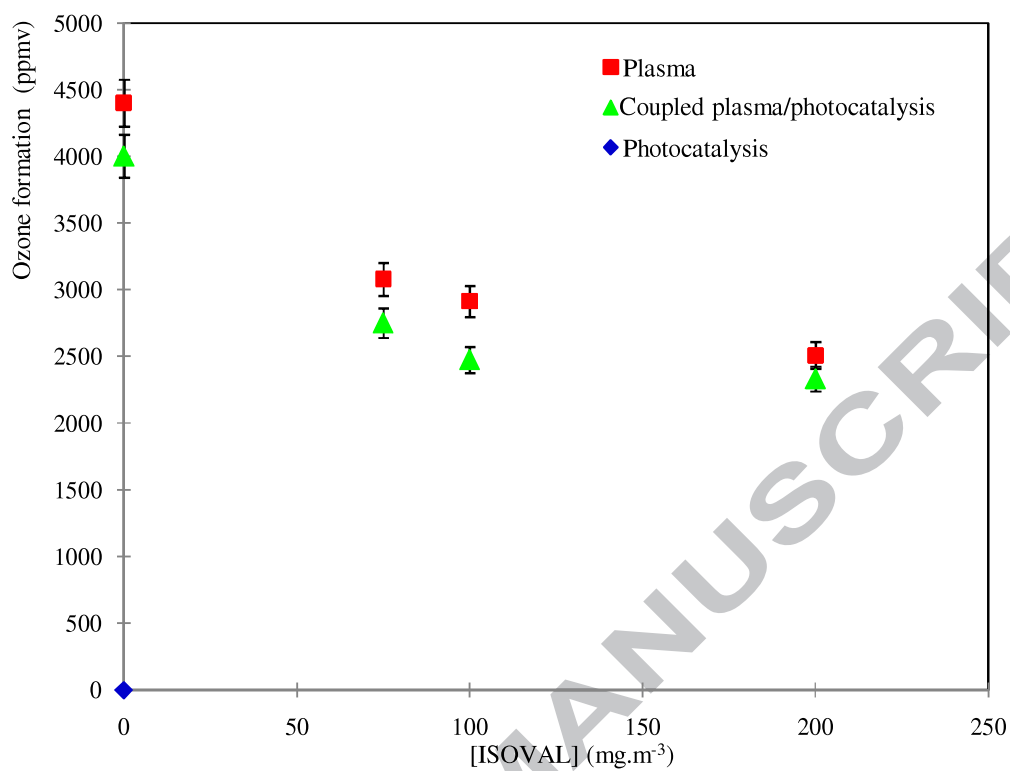
944

945

946

947

948



949

950

951 Fig. 8: Variation of the amount of ozone with inlet concentration using three processes (SE =

952

17 J.L⁻¹, Q = 2 m³.h⁻¹, T = 20 °C, RH = 5%, I = 20 W.m⁻²).

953

954

955

956

957

958

959

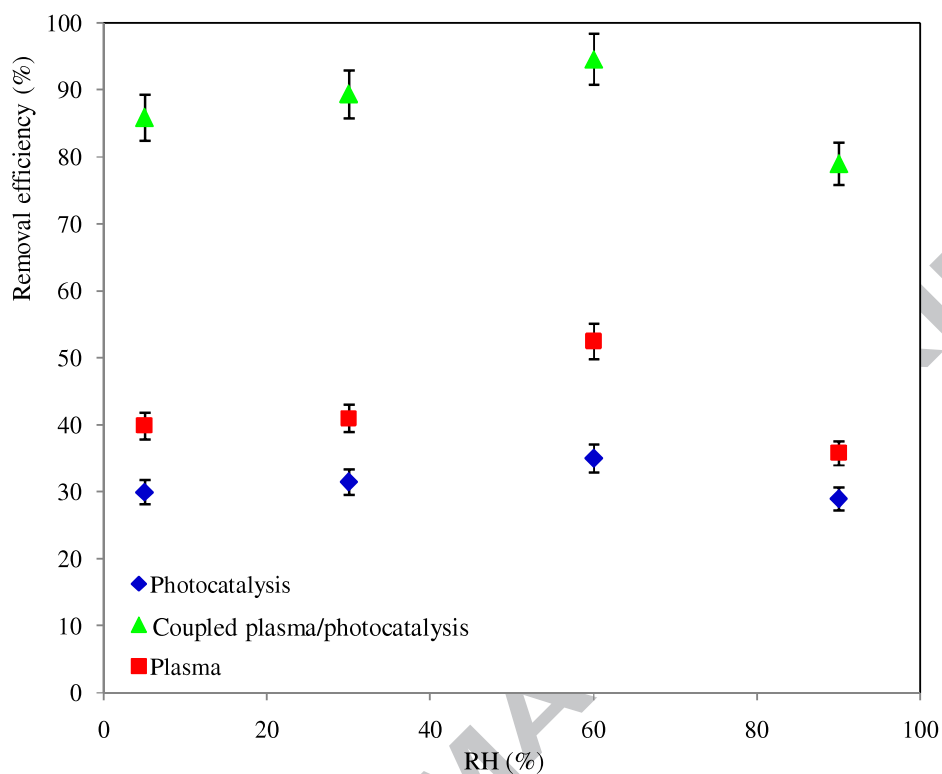
960

961

962

963

964



965

966 Fig. 9: Variation of isovaleraldehyde removal efficiency vs. RH using three processes

967 ($[\text{ISOVAL}]_0 = 100 \text{ mg/m}^3$, $Q = 2 \text{ m}^3 \cdot \text{h}^{-1}$, $T = 20 \text{ }^\circ\text{C}$, $SE = 17 \text{ J} \cdot \text{L}^{-1}$, $I = 20 \text{ W} \cdot \text{m}^{-2}$).

968

969

970

971

972

973

974

975

976

977

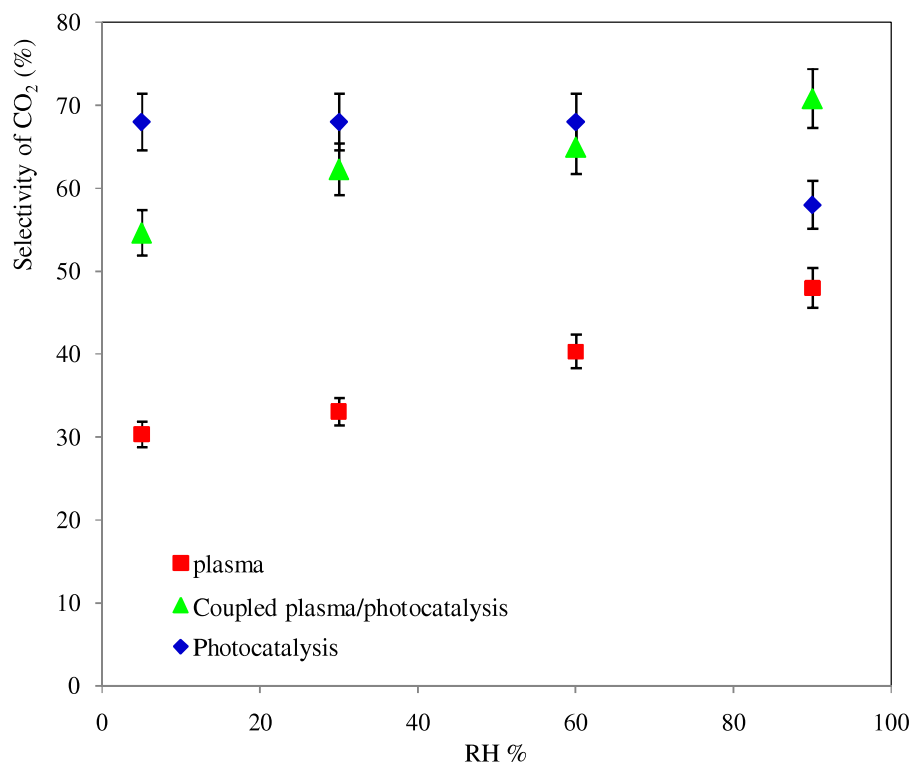
978

979

980

981

982



983

984

Fig. 10: Variation of the selectivity of CO₂ vs. RH

985

([ISOVAL] = 100 mg. m⁻³, Q = 2 m³.h⁻¹, T = 20 °C, SE = 17 J.L⁻¹, I = 20 W. m⁻²).

986

987

988

989

990

991

992

993

994

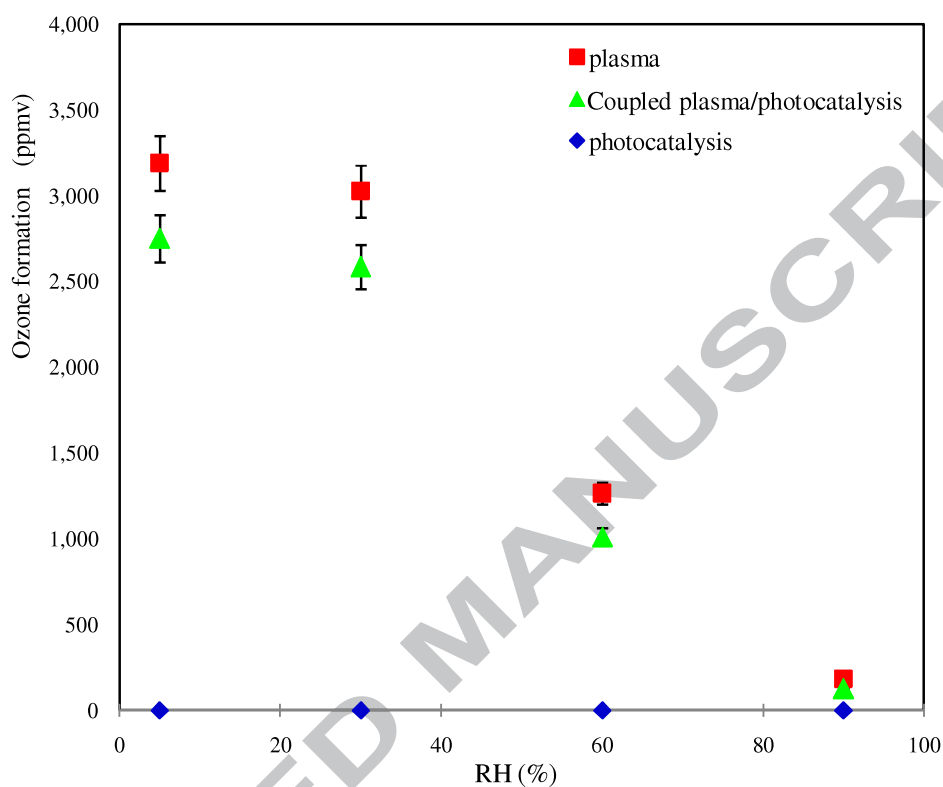
995

996

997

998

999



1000

1001 Fig. 11: Variation of the amount of ozone with relative humidity using three processes

1002 ([ISOVAL] = 100 mg. h⁻¹, Q = 2 m³.h⁻¹, T = 20 °C, SE = 17 J.L⁻¹, I = 20 W. m⁻²).

1003

1004

1005

1006

Highlights:

1007

1008

Isovaleraldehyde elimination by DBD plasma and photocatalysis is studied.

1009

Effects of some operating parameters on performance of each process are tested.

1010

A synergetic effect is observed by coupling plasma DBD and photocatalysis.

1011

The byproducts of isovaleraldehyde are identified and evaluated.

1012

A possible pathway of Isovaleraldehyde removal is proposed.

1013

1014

ACCEPTED MANUSCRIPT